AAS 01-417

RELATIVE EQUILIBRIA OF A GYROSTAT WITH A DISCRETE DAMPER *

Ralph A. Sandfry † and Christopher D. Hall‡

We investigate the possible equilibria for a torque-free gyrostat with an attached spring-mass damper. The equations of motion are presented as well as explicit stability conditions for simple spins. We numerically determine additional equilibria using numerical continuation and rotor momentum as the bifurcation parameter. Multiple equilibria are presented, including stable equilibria corresponding to steady spins in non-trivial directions. A pitchfork bifurcation of the nominal-spin state is examined analytically using Liapunov-Schmidt reduction, which produces conditions on system parameters for avoiding a jump phenomenon.

INTRODUCTION

The stability of spinning satellites depends on how energy dissipation is used to effectively damp out perturbations from the desired spin. However, energy dissipation can significantly affect the stability conditions for spinning satellites. Whereas an undamped, spinning rigid body is stable in spins about either a major or minor axis, the presence of energy dissipation destabilizes a minor-axis spin. Although this result was known to some researchers,[1] it was unexpectedly demonstrated with Explorer I.[2] Dual-spin satellites were developed to gyroscopically stabilize the intended spin, even about a minor axis. The dual-spin concept includes a single, axisymmetric rotor, with the rotor spin-axis aligned with the satellite spin-axis, and a despun or slowly spinning platform. Researchers often model a dual-spin satellite as a rigid body with a rotor, called a gyrostat. We refer to gyrostats designed to spin about the minor axis as prolate, whereas major-axis gyrostats are denoted oblate. The most common configuration is prolate, which allows a stable, minor-axis spin.

---

†PhD Candidate, Aerospace and Ocean Engineering, Virginia Polytechnic Institute and State University, Blacksburg, Virginia, 24061. Member AIAA. Member AAS.

‡Associate Professor, Aerospace and Ocean Engineering, Virginia Polytechnic Institute and State University, Blacksburg, Virginia 24061. Associate Fellow AIAA. Member AAS.

Much work went into ensuring that prolate dual-spin satellites can be stable even in the presence of energy dissipation. Approximate energy-sink methods were used to develop useful stability criteria for the nominal-spin equilibrium state.[3–5] Other researchers analyzed the full system of equations including specific damping devices which complicated the stability analysis.[5–9] In general, the energy-sink methods provide useful results, but more precise stability conditions are possible by including specific damping devices in the model and analyzing the full system of equations. Hughes[10] has used both energy sink methods and discrete damper models to generate stability conditions for rigid bodies and gyrostats. The vast majority of work has focused on the stability of the nominal spin, whereas few have examined other possible equilibria.

Some researchers have studied multiple equilibria for spinning rigid bodies with energy dissipation.[11,12] Chinnery and Hall[13] obtained new results on the bifurcations in equilibria that occur for a rigid body with a discrete damper situated in a principal plane and aligned parallel to the nominal spin axis (the major axis). Hall[14] reviewed the equations of motion for an N-rotor gyrostat with a discrete damper and the stability conditions for a single-rotor version. In an earlier paper,[15] we obtained some new results on the bifurcations in equilibria that occur for a gyrostat with a discrete damper situated in a principal plane and aligned parallel to the nominal spin axis (the major axis). The equilibria and bifurcations considered in this earlier work were all within a principal plane of the system. The purpose of the present paper is to present the results of applying numerical continuation to generate global equilibria in the full state space and bifurcation diagrams for a prolate gyrostat with a discrete damper. We use numerical continuation theory to generate bifurcation diagrams and examine the more complete set of equilibria for prolate gyrostats.

MODEL AND EQUATIONS OF MOTION

The model we study is shown in Figure 1, consisting of a rigid body, $\mathcal{B}$, containing a rigid axisymmetric rotor, $\mathcal{R}$, and a mass particle $\mathcal{P}$, which is constrained to move along a line $\hat{\mathbf{n}}$ fixed in $\mathcal{B}$. A rigid body with damper is denoted $\mathcal{B}+\mathcal{P}$ while the gyrostat with damper is $\mathcal{B}+\mathcal{R}+\mathcal{P}$. The body frame has origin $\mathcal{O}$ and axes $\hat{\mathbf{b}}_i$ are system principal axes when $\mathcal{P}$ is in its rest position ($x^*=0$). The vector $\hat{\mathbf{n}}$ is parallel to $\hat{\mathbf{b}}_1$, which is the nominal-spin axis for the spacecraft. The particle is connected to a linear spring and has linear damping. The rotor spin-axis is in the $\hat{\mathbf{a}}$ direction, parallel to the $\hat{\mathbf{b}}_1$ axis. All vectors and tensors are expressed with respect to the body frame. This configuration is a reasonable model for a dual-spin spacecraft with a "ball-in-tube" type precession damper. It also can model any spacecraft with a single momentum wheel and a similar damper. In a more general sense, the damper properties may be adjusted to model a flexible appendage attached to the rigid body.

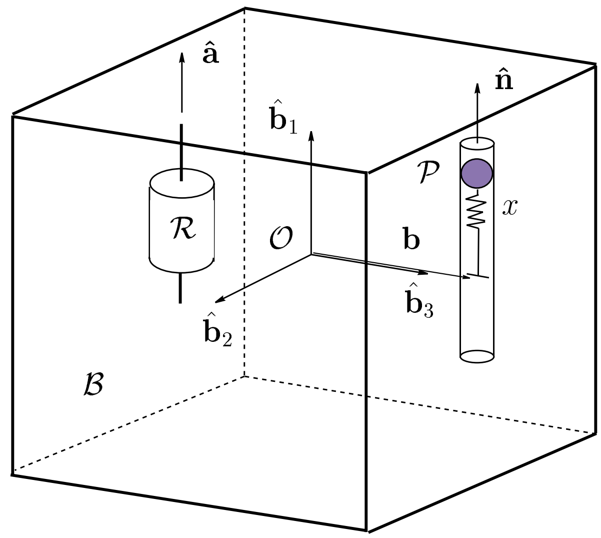

Figure 1: Single-rotor axial gyrostat with aligned discrete damper

The equations of motion are developed by Hughes[10] in dimensional form using a Newton-Euler approach. The system linear and angular momenta are denoted $\mathbf{p}^*$ and $\mathbf{h}^*$ respectively, where the asterisk is used to indicate dimensional quantities. The linear momentum of the damper mass in the $\hat{\mathbf{n}}$ direction is p_n^* and the relative displacement and velocity of the damper mass in the $\hat{\mathbf{n}}$ direction are x^* and y^*. The position vector from $\mathcal{O}$ to $\mathcal{P}$ is $\mathbf{r}_p^* = \mathbf{b}^* + x^*\mathbf{n}$ where $\mathbf{b}^*$ is a vector from $\mathcal{O}$ to the undeformed position of the damper mass. The angular velocity of the body frame with respect to the inertial frame is $\boldsymbol{\omega}^*$. The origin of the body frame, point $\mathcal{O}$, has velocity $\mathbf{v}_o^*$. The rotor angular momentum component along the rotor axis of symmetry *relative to the platform*, is $\mathbf{h}_s^* = \hat{\mathbf{a}} I_s^* \omega_s^* \stackrel{\triangle}{=} \hat{\mathbf{a}} h_s^*$. The symbol I_s^* denotes the rotor axial moment of inertia and ω_s^* is the rotor angular speed relative to the platform. The rotor is subject to axial torque g_a^* applied by the platform. The *absolute* rotor angular momentum is $h_a^* = I_s^* \hat{\mathbf{a}}^T \boldsymbol{\omega}^* + h_s^* = I_s^*(\hat{\mathbf{a}}^T \boldsymbol{\omega}^* + \omega_s^*)$. The mass of the damper particle is m_d^* and the total system mass is m^*. The system inertia matrix is $\mathbf{I}^*$ which depends on x^*. The moment of inertia when the particle is not deflected is $\mathbf{I}_o^*$. The spring has stiffness k^* and the damper has damping coefficient c_d^*. The external force and moment are $\mathbf{f}^*$ and $\mathbf{g}^*$. Using these definitions, we present the equations of motion in the following section in dimensional form.

Dimensional Equations of Motion

The equations of motion for the gyrostat with discrete damper are:

$$\begin{aligned}
\dot{\mathbf{p}}^* &= -\boldsymbol{\omega}^{*\times}\mathbf{p}^* + \mathbf{f}^* && (1)\\
\dot{\mathbf{h}}^* &= -\boldsymbol{\omega}^{*\times}\mathbf{h}^* - \mathbf{v}_o^{*\times}\mathbf{p}^* + \mathbf{g}^* && (2)\\
\dot{p}_n^* &= m_d^*\boldsymbol{\omega}^{*\mathrm{T}}\hat{\mathbf{n}}^\times\left[\mathbf{v}_o^* - (\mathbf{b} + x^*\hat{\mathbf{n}})^\times\boldsymbol{\omega}^*\right] - c_d^* y^* - k^* x^* && (3)\\
\dot{h}_a^* &= g_a^* && (4)\\
\dot{x}^* &= y^* && (5)
\end{aligned}$$

The superscript $\times$ denotes the skew-symmetric matrix form of a vector.[10] The system momenta are:

$$\begin{aligned}
\mathbf{p}^* &= m^*\mathbf{v}^*{}_o - m_d^* x^*\hat{\mathbf{n}}^\times\boldsymbol{\omega}^* + m_p^* y^*\hat{\mathbf{n}} && (6)\\
\mathbf{h}^* &= m_d^* x^*\hat{\mathbf{n}}^\times\mathbf{v}_o^* + \mathbf{I}^*\boldsymbol{\omega}^* + m_d^* y^*\mathbf{b}^{*\times}\hat{\mathbf{n}} + \mathbf{h}_s^* && (7)\\
p_n^* &= m_d^*\left(\hat{\mathbf{n}}^\mathrm{T}\mathbf{v}_o^* - \hat{\mathbf{n}}^\mathrm{T}\mathbf{b}^{*\times}\boldsymbol{\omega}^* + y^*\right) && (8)\\
h_a^* &= I_s^*\hat{\mathbf{a}}^\mathrm{T}\boldsymbol{\omega}^* + I_s^*\omega_s^* && (9)
\end{aligned}$$

and the inertia matrix is:

$$\mathbf{I}^* = \mathbf{I}_o^* + m_d^*\left[\left(2x^*\mathbf{b}^{*\mathrm{T}}\hat{\mathbf{n}} + x^{*2}\right)\mathbf{1} - x^*\left(\mathbf{b}^*\hat{\mathbf{n}}^\mathrm{T} + \hat{\mathbf{n}}\mathbf{b}^{*\mathrm{T}}\right) - x^{*2}\hat{\mathbf{n}}\hat{\mathbf{n}}^\mathrm{T}\right] \qquad (10)$$

The equations of motion consist of nine ordinary differential equations. These equations are non-dimensionalized prior to any simplification or analysis. Whereas the dimensional quantities are denoted with an asterisk, the asterisk is dropped for the equivalent dimensionless quantities.

Dimensionless Equations of Motion

The full equations are made dimensionless by defining characteristic length, mass, and time units. These quantities are used to non-dimensionalize the variables and parameters of the problem. Many possible characteristic quantities are possible, but certain quantities lead to equations with desirable qualities. We prefer characteristic quantities that allow satellites with the same dimensional inertia properties to have the same non-dimensional inertia properties. If we select damper parameters as characteristic quantities, then the same satellite with two different dampers would have different non-dimensional inertia properties. We want to avoid this difference so we choose characteristic values without damper parameters.

We select the following characteristic quantities,

$$
\begin{aligned}
\text{Length} &= \sqrt{\mathrm{tr}\,\mathbf{I}_0{}^*/m^*} \\
\text{Mass} &= m^* \\
\text{Time} &= \mathrm{tr}\,\mathbf{I}_0{}^*/h^*
\end{aligned}
$$

These definitions produce equations with two notable features: the trace of the dimensionless inertia matrix is always one, $\mathrm{tr}\,\mathbf{I}_0 = 1$, and the dimensionless angular momentum vector also has unit length, $\mathbf{h}^{\mathrm{T}}\mathbf{h} = 1$. This latter feature is only true if $\mathbf{g} = \mathbf{0}$.

The following relationships are used to make the full equations dimensionless:

$$
\begin{array}{cc}
\mathbf{p}^* = \left(h^*\sqrt{m^*/\mathrm{tr}\,\mathbf{I}_0{}^*}\right)\mathbf{p} & \mathbf{h}^* = h^*\mathbf{h} \\
p_n^* = \left(h^*\sqrt{m^*/\mathrm{tr}\,\mathbf{I}_0{}^*}\right)p_n & \mathbf{v}_o^* = \left(h^*/\sqrt{m^*\mathrm{tr}\,\mathbf{I}_0{}^*}\right)\mathbf{v}_o \\
\boldsymbol{\omega}^* = \left(h^*/\mathrm{tr}\,\mathbf{I}_0{}^*\right)\boldsymbol{\omega} & y^* = \left(h^*/\sqrt{m^*\mathrm{tr}\,\mathbf{I}_0{}^*}\right)y \\
x^* = \left(\sqrt{\mathrm{tr}\,\mathbf{I}_0{}^*/m^*}\right)x & \boldsymbol{\omega}_s^* = \left(h^*/\mathrm{tr}\,\mathbf{I}_0{}^*\right)\boldsymbol{\omega}_s \\
t^* = \left(\mathrm{tr}\,\mathbf{I}_0{}^*/h^*\right)t & \mathbf{h}_a^* = h^*\mathbf{h}_a \\
\mathbf{b}^* = \left(\sqrt{\mathrm{tr}\,\mathbf{I}_0{}^*/m^*}\right)\mathbf{b} & m_d^* = \varepsilon m^* \\
\mathbf{I}^* = \mathrm{tr}\,\mathbf{I}_0{}^*\mathbf{I} & \mathbf{I}_s^* = \mathrm{tr}\,\mathbf{I}_0{}^*\mathbf{I}_s \\
c_d^* = \left(m^*h^*/\mathrm{tr}\,\mathbf{I}_0{}^*\right)c_d & k^* = \left(m^*h^{*2}/\mathrm{tr}\,\mathbf{I}_0{}^{*2}\right)k \\
\dot{\mathbf{p}}^* = \left(h^{*2}\sqrt{m^*/\mathrm{tr}\,\mathbf{I}_0{}^{*3}}\right)\dot{\mathbf{p}} & \dot{\mathbf{h}}^* = \left(h^{*2}/\mathrm{tr}\,\mathbf{I}_0{}^*\right)\dot{\mathbf{h}}
\end{array}
\tag{11}
$$

Substituting these expressions into the dimensional equations results in the following dimensionless equations of motion

$$\dot{\mathbf{p}} = -\boldsymbol{\omega}^\times\mathbf{p} + \mathbf{f} \tag{12}$$

$$\dot{\mathbf{h}} = -\boldsymbol{\omega}^\times\mathbf{h} - \mathbf{v}_o^\times\mathbf{p} + \mathbf{g} \tag{13}$$

$$\dot{h}_a = g_a \tag{14}$$

$$\dot{p}_n = \varepsilon\boldsymbol{\omega}^T\hat{\mathbf{n}}^\times[\mathbf{v}_o - (\mathbf{b} + x\hat{\mathbf{n}})^\times\boldsymbol{\omega}] - c_d y - kx \tag{15}$$

$$\dot{x} = y \tag{16}$$

with dimensionless system momenta

$$\mathbf{p} = \mathbf{v}_o - \varepsilon x\hat{\mathbf{n}}^\times\boldsymbol{\omega} + \varepsilon y\hat{\mathbf{n}} \tag{17}$$

$$\mathbf{h} = \mathbf{I}\boldsymbol{\omega} + \varepsilon x\hat{\mathbf{n}}^\times\mathbf{v}_o + \varepsilon y\mathbf{b}^\times\hat{\mathbf{n}} + I_s\omega_s\hat{\mathbf{a}} \tag{18}$$

$$h_a = I_s(\hat{\mathbf{a}}^T\boldsymbol{\omega} + \omega_s) \tag{19}$$

$$p_n = \varepsilon(\hat{\mathbf{n}}^T\mathbf{v}_o - \hat{\mathbf{n}}^T\mathbf{b}^\times\boldsymbol{\omega} + y) \tag{20}$$

The dimensionless moment of inertia matrix is

$$\mathbf{I} = \mathbf{I}_o + \varepsilon\left[\left(2x\mathbf{b}^T\hat{\mathbf{n}} + x^2\right)\mathbf{1} - x(\mathbf{b}\hat{\mathbf{n}}^T + \hat{\mathbf{n}}\mathbf{b}^T) - x^2\hat{\mathbf{n}}\hat{\mathbf{n}}^T\right] \tag{21}$$

In the next section, we reduce the order of the system equations by several simplifying assumptions.

Reduced Order Equations of Motion

We make several assumptions, consistent with the intention of studying the free motion of the damped gyrostat, which simplify the equations of motion. We assume $\mathbf{f} = \mathbf{g} = \mathbf{0}$ and $g_a = 0$. Thus, $\mathbf{p}$ and $\mathbf{h}$ have constant magnitude as they are constant in inertial space. We assume, without loss of generality, that $\mathbf{p} = \mathbf{0}$. Furthermore, h_a is constant, and we treat is as a bifurcation parameter instead of as a dynamic variable. With these assumptions, we can solve for the velocity:

$$\mathbf{v}_o = \varepsilon x \hat{\mathbf{n}}^{\times} \boldsymbol{\omega} - \varepsilon y \hat{\mathbf{n}}$$

Substituting for $\mathbf{v}_o$ in the expression for angular momentum, we can solve for the angular velocity

$$\boldsymbol{\omega} = \mathbf{K}^{-1}\mathbf{m}$$

by defining $\varepsilon' = 1 - \varepsilon$, and

$$\begin{aligned}
\mathbf{K} &= \mathbf{I}_o - I_s \hat{\mathbf{a}}\hat{\mathbf{a}}^{\mathrm{T}} + \varepsilon \left[2x\mathbf{b}^{\mathrm{T}}\hat{\mathbf{n}}\mathbf{1} - x(\mathbf{b}\hat{\mathbf{n}}^{\mathrm{T}} + \hat{\mathbf{n}}\mathbf{b}^{\mathrm{T}}) - \varepsilon' x^2 \hat{\mathbf{n}}^{\times}\hat{\mathbf{n}}^{\times} \right] \\
\mathbf{m} &= \mathbf{h} - h_a \hat{\mathbf{a}} - \varepsilon y \mathbf{b}^{\times}\hat{\mathbf{n}}
\end{aligned}$$

Given the stated assumptions and eliminating the velocities from the equations of motion reduces the system to five scalar equations in $\mathbf{h}$, p_n, and x:

$$\dot{\mathbf{h}} = \mathbf{h}^{\times}\mathbf{K}^{-1}\mathbf{m} \tag{22}$$

$$\dot{p}_n = -\varepsilon \mathbf{m}^{\mathrm{T}}\mathbf{K}^{-1}\hat{\mathbf{n}}^{\times} \left[(\mathbf{b} + \varepsilon' x \hat{\mathbf{n}})^{\times} \mathbf{K}^{-1}\mathbf{m} \right] - c_d y - kx \tag{23}$$

$$\dot{x} = y \tag{24}$$

where

$$\varepsilon y = \frac{p_n + \varepsilon \hat{\mathbf{n}}^{\mathrm{T}}\mathbf{b}^{\times}\mathbf{K}^{-1}(\mathbf{h} - h_a\hat{\mathbf{a}})}{\varepsilon' + \varepsilon \hat{\mathbf{n}}^{\mathrm{T}}\mathbf{b}^{\times}\mathbf{K}^{-1}\mathbf{b}^{\times}\hat{\mathbf{n}}} \tag{25}$$

These equations are used in the numerical and analytical studies in this paper.

Comments on Equations of Motion

A related problem to the gyrostat with discrete damper (identified as $\mathcal{B} + \mathcal{R} + \mathcal{P}$) is the rigid body with discrete damper (identified as $\mathcal{B} + \mathcal{P}$). Chinnery and Hall[13] developed equations of motion for the $\mathcal{B} + \mathcal{P}$ model, configured as the previously defined nominal configuration but without the rotor. The equations for the $\mathcal{B}+\mathcal{R}+\mathcal{P}$ case can be reduced to those for the $\mathcal{B} + \mathcal{P}$ case by the transformation

$$(h_a, I_1') \mapsto (0, I_1) \tag{26}$$

Therefore, results obtained for $h_a = 0$ are applicable to the $\mathcal{B}+\mathcal{P}$ case and comparable to previous results by Chinnery and Hall.

The equivalence defined by Eq. (26) does not imply the rotor is fixed. It does imply that the dynamics of the $\mathcal{B}+\mathcal{R}+\mathcal{P}$ system, with $h_a = 0$, are the same as the $\mathcal{B}+\mathcal{P}$ system, but for a different inertia matrix. For $h_a = 0$, the rotor velocity relative to the rigid body is

$$\omega_s = -\hat{\mathbf{a}}^{\mathrm{T}}\boldsymbol{\omega} \tag{27}$$

The rotor will rotate in an opposite sense relative to the contribution of $\boldsymbol{\omega}$ in order to maintain the *absolute* angular momentum of zero, in the absence of any rotor torques. A fixed rotor is characterized by $h_s = 0$, and equations reduce to those for the $\mathcal{B}+\mathcal{P}$ model.

Since the system is free of external torques, system angular momentum is conserved. In general terms of the state vector, $\mathbf{z} = (h_1, h_2, h_3, p_n, x)$, a conserved quantity takes the form,

$$C(\mathbf{z}) = 0$$

which for conserved angular momentum becomes

$$h_1^2 + h_2^2 + h_3^2 - 1 = 0 \tag{28}$$

This constraint between the states has the effect of a persistent zero eigenvalue in the system Jacobian matrix. A singular Jacobian affects how we can achieve the objective of characterizing the possible system equilibria using numerical continuation.

Instead of using the conserved quantity to eliminate one of the states, we change variables to spherical coordinates. The conserved magnitude of the angular momentum vector, denoted as h, forces all possible states to lie on a momentum sphere of radius h. As such, the three state variables representing the angular momentum vector, (h_1, h_2, h_3), can be expressed in spherical coordinates, (h, θ, ϕ). By converting the state from (h_1, h_2, h_3, p_n, x) to $(h, \theta, \phi, p_n, x)$, we effectively reduce the system to four first-order equations. This reduction is possible because, in terms of these variables, the conserved quantity itself becomes a state, and $\dot{h} = 0$ by definition. We convert Eqs. (23–24) to the new variables by simply substituting for $\mathbf{h}$. To convert Eq. (22) to the new variables requires use of a transformation matrix derived from the spherical coordinate definitions. Similar to kinematic expressions for Euler angle rates, no one set of spherical-angle definitions is non-singular for the entire state space. However, by choosing the transformation appropriately, the singularity can be placed in an unimportant region of state space. Being aware of the singularity, we can use an alternate transformation if numerical problems occur when working in regions of state space near the original transformation's singularity. Using the spherical coordinate representation of the system equations, we use numerical continuation to explore the possible system equilibria. Before discussing this analysis, we review the explicit stability conditions for simple spins.

STABILITY OF SIMPLE SPINS

The most useful relative equilibrium condition for this model corresponds to a steady spin about the $\hat{\mathbf{b}}_1$ axis. For this equilibrium, the damper is not deflected and there is no damper momentum in the $\hat{\mathbf{n}}$ direction, $(x = p_n = 0)$. After linearizing the reduced, non-dimensional equations of motion about the state $(\mathbf{h}, p_n, x) = (1, 0, 0, 0, 0)$, Routh-Hurwitz stability criteria (Ref. 10) are applied to produce the known linearized stability conditions:[14]

$$
\begin{aligned}
I_1' &> -\max(I_2, I_3)\lambda && (29)\\
k &> -(b^2\varepsilon^2\lambda^3)/\left[I_1'^2(I_1' + I_3\lambda)\right] && (30)
\end{aligned}
$$

where $I_1' = I_1 - I_s$ and $\lambda = h_a - 1$.

These conditions verify that for $h_a = 0$ and sufficiently large spring stiffness, steady spins about the major axis are stable. These results agree with stability conditions derived for rigid bodies with the same damper mechanism.[13] Non-zero wheel momentum alters the stability conditions, but qualitatively the results are similar: for a specific damper location and wheel momentum there is a critical spring constant below which the equilibrium is unstable. For a prolate gyrostat, with $I_1' < \min(I_2, I_3)$, a stable nominal spin requires $h_a > 0$.

Steady spins are also possible about the other two axes, $\hat{\mathbf{b}}_2$ and $\hat{\mathbf{b}}_3$ when $h_a = 0$. These spins correspond to a rigid body with a damper mounted perpendicular to the spin axis. The effectiveness of this damper configuration (denoted a nutation damper) was compared with a damper aligned with the spin axis (denoted a precession damper) by Schneider and Likins who found that in general the precession damper was more effective.[16] The spin about the $\hat{\mathbf{b}}_2$ axis may be characterized by a zero or non-zero damper deflection. Sandfry derived stability conditions for the $\hat{\mathbf{b}}_2$-axis spin with $x = 0$ and the $\hat{\mathbf{b}}_3$-axis spin.[17] For the $\hat{\mathbf{b}}_2$-axis spin, with $h_a = x = 0$, a linear analysis is inconclusive, so the stability conditions are determined with a Liapunov stability analysis:

$$
\begin{aligned}
I_2 &> \max\left(I_1', I_3\right) && (31)\\
k &> \varepsilon\varepsilon'/I_2^2 && (32)
\end{aligned}
$$

For the $\hat{\mathbf{b}}_3$-axis spin Sandfry used a linear stability analysis to determine the following stability conditions:

$$
\begin{aligned}
I_3 &> \max(I_1', I_2) && (33)\\
k &> \frac{b^2\varepsilon^2 + \varepsilon\varepsilon'(I_3 - I_1')}{{I_3}^2(I_3 - I_1')} && (34)
\end{aligned}
$$

In both cases, a major-axis rule applies. Without gyroscopic stabilization, the spins are only stable about a major axis. The advantage of including the damper in the model is revealed by the additional requirement: the spring must be sufficiently stiff to ensure a stable spin. As pointed out by Hughes, using only an energy sink approximation for damping leads to a major-axis rule, but including the damper in the model provides more precise stability conditions.[10]

As I_1' is the critical moment of inertia about the $\hat{\mathbf{b}}_1$ axis for stability purposes, we make our definitions for prolate and oblate more precise by defining a gyrostat with $I_1' < \min(I_2, I_3)$ as prolate. A gyrostat with $I_1' > \max(I_2, I_3)$ is defined as oblate.

BIFURCATIONS OF EQUILIBRIA

Equilibrium values of $\mathbf{h}$, h_a, p_n and x are found by setting Eqs. (22–24) equal to zero and solving the resulting algebraic equations. By linearizing these equations about the equilibrium point, the local stability of the equilibrium is found by examining the eigenvalues of the resulting Jacobian. Multiple equilibrium solutions often exist for the same values of the system parameters. Changing key system parameters, such as b, k or h_a may produce significantly different equilibria. Plotting equilibrium points while varying a system parameter generates a bifurcation diagram. Critical equilibrium points may exist where the number of equilibria changes, or bifurcates. Bifurcations are often classified by the structure of the bifurcation diagram near these bifurcation points. Many references exist on bifurcation classification and theory, including Refs. 18 and 19. To investigate the possible equilibrium motions we start from a known equilibrium point and generate bifurcation diagrams numerically using the AUTO[20] continuation program. The process is complicated by the conserved angular momentum which produces a zero eigenvalue in the Jacobian at all equilibrium points. Using the spherical coordinate representation of the system equations, we use numerical continuation to generate bifurcation diagrams. The equilibria are converted back to the original states, $\mathbf{z} = (h_1, h_2, h_3, p_n, x)$, and plotted to create bifurcation diagrams.

Another useful graphical representation is to plot the equilibria in (h_1, h_2, h_3) momentum space. With the conserved angular momentum, all equilibria lie on the momentum sphere of radius $h = 1$. Examining Eq. (22), we find that at equilibrium, the angular momentum and velocity vectors are parallel. Therefore, the equilibria on the momentum sphere identify the direction in the body frame of the equilibrium spin axis.

As an initial example, we investigate the equilibria for a gyrostat with the following system parameters: $\mathbf{I} = \mathrm{diag}(0.28, 0.32, 0.40)$, $I_s = 0.04$, $\varepsilon = 0.1$, $c_d = 0.1$, $b = 0.5$, and $k = 0.4$. We apply numerical continuation to this system while allowing rotor momentum, h_a to vary as the bifurcation parameter. The equilibria for this example are displayed on the momentum sphere and in bifurcation diagrams in Figure 2. For all these diagrams, solid lines represent stable equilibria, and dashed lines

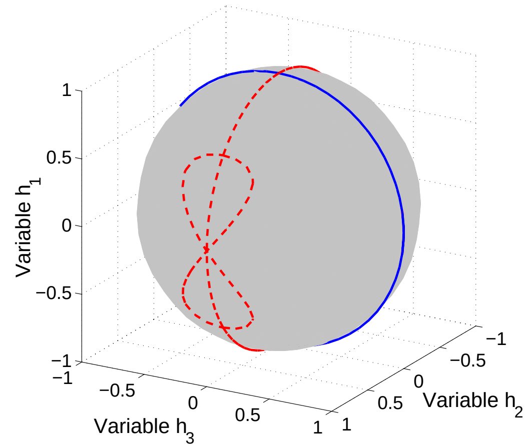

(a) Equilibria on the momentum sphere for varying h_a

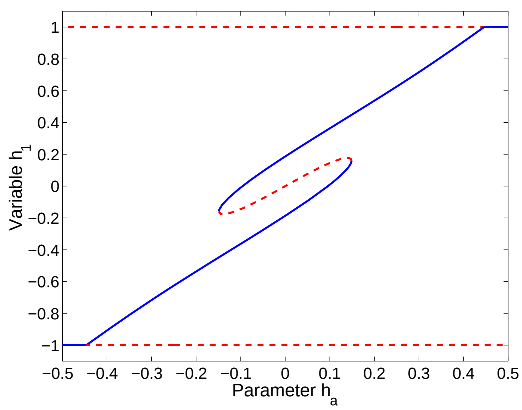

(b) Bifurcation diagram for equilibria within the $\hat{\mathbf{b}}_1$–$\hat{\mathbf{b}}_3$ plane: h_1 *vs.* h_a

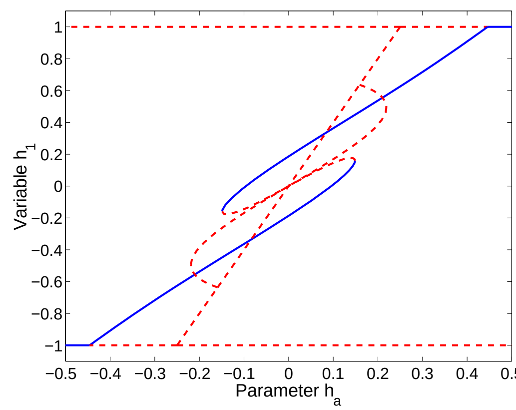

(c) Bifurcation diagram for full equilibria: h_1 *vs.* h_a

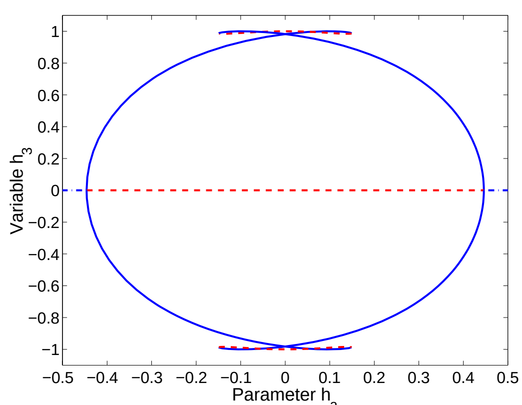

(d) Bifurcation diagram for equilibria within the $\hat{\mathbf{b}}_1$–$\hat{\mathbf{b}}_3$ plane: h_3 *vs.* h_a

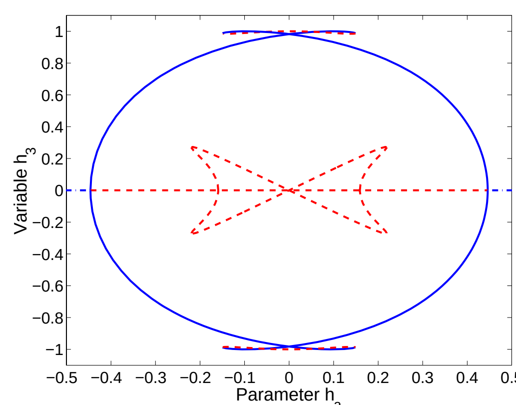

(e) Bifurcation diagram for full equilibria: h_3 *vs.* h_a

Figure 2: Equilibria for prolate gyrostat with $I_2 < I_3$, $k = 0.4$

indicate unstable equilibria. The nominal spin state is a single point on the top of the momentum sphere, at $\mathbf{h} = (1, 0, 0)$. Additional branches of equilibria bifurcate from this nominal spin condition into the $\hat{\mathbf{b}}_1$–$\hat{\mathbf{b}}_2$ and $\hat{\mathbf{b}}_1$–$\hat{\mathbf{b}}_3$ planes, as seen in Figure 2(a). Equilibria also bifurcate from the $\hat{\mathbf{b}}_1$–$\hat{\mathbf{b}}_2$ plane, forming branches that do not lie in any body-frame plane. The branches do not actually intersect at $\mathbf{h} = (0, 1, 0)$ because the equilibria differ in the remaining damper states. The only stable equilibria are certain nominal spins and some equilibria within the $\hat{\mathbf{b}}_1$–$\hat{\mathbf{b}}_3$ plane.

Figure 2(b) shows the h_1–h_a bifurcation diagram of branches in the $\hat{\mathbf{b}}_1$–$\hat{\mathbf{b}}_3$ plane. Figure 2(c) is the complete bifurcation diagram, including the branches in the $\hat{\mathbf{b}}_1$–$\hat{\mathbf{b}}_2$ plane and out of plane. The nominal spin equilibria, with $h_1 = +1$, is clearly seen in these bifurcation diagrams for varying h_a. The stability changes from unstable to stable as h_a increases past the threshold defined by the stability condition, Eq. (30). Figures 2(d) and 2(e) show the h_3–h_a bifurcation diagrams. In these latter diagrams, the nominal-spin bifurcation points are pitchfork bifurcations. Also, the dash-dot lines indicate the existence of stable and unstable branches for the same value of variable and bifurcation parameter. In this example, the $h_3 = 0$ axis includes both branches of $\hat{\mathbf{b}}_1$-axis spins, $\mathbf{h} = (\pm 1, 0, 0)$.

The stability conditions for the nominal spin define the bifurcation points where new branches emanate from the branches of nominal-spin equilibria. In general, the stability conditions define points where eigenvalues of the system Jacobian cross the imaginary axis. At such points, the Jacobian is singular and may indicate a bifurcation point. Equation (29) depends only on $\mathbf{I}$, I_s and h_a, and defines the bifurcation value of h_a for branches bifurcating into the $\hat{\mathbf{b}}_1$–$\hat{\mathbf{b}}_2$ plane. Equation (30) depends on $\mathbf{I}$, I_s, h_a and the damper parameters k, b, and ε. For given inertia properties and damper parameters, the stability threshold defines the bifurcation value of h_a for branches bifurcating into the $\hat{\mathbf{b}}_1$–$\hat{\mathbf{b}}_2$ plane.

For prolate gyrostats with $I_2 > I_3$, the equilibria and their stability are significantly different from the $I_3 > I_2$ case shown in Figure 2. Figure 3 shows the equilibria and bifurcation diagrams for a system with the same parameters as Figure 2, but with $\mathbf{I} = \mathrm{diag}(0.28, 0.40, 0.32)$. Changing the major axis has important stability implications. The $\hat{\mathbf{b}}_1$–$\hat{\mathbf{b}}_3$ plane equilibria are all unstable with the exception of nominal spins with sufficient rotor momentum, as seen in Figure 3(b). Some stable and unstable equilibria occur in the $\hat{\mathbf{b}}_1$–$\hat{\mathbf{b}}_2$ plane. The bifurcation point within the $\hat{\mathbf{b}}_1$–$\hat{\mathbf{b}}_2$ plane has stable pitchfork branches that bifurcate out of plane, as seen in Figures 3(a) and 3(c). These stable, out-of-plane equilibria are interesting possible trap states for gyrostats with free-spinning rotors when perturbed from the intended spin.

We next consider the effects of varying spring stiffness, focusing on the $I_3 > I_2$ version of a prolate gyrostat. Decreasing k affects the global equilibria, as shown in Figure 4. Out-of-plane equilibria become more pronounced, with larger h_3 magnitude, and approach the $\hat{\mathbf{b}}_1$–$\hat{\mathbf{b}}_3$ plane, as shown in Figure 4(c). For some value of spring

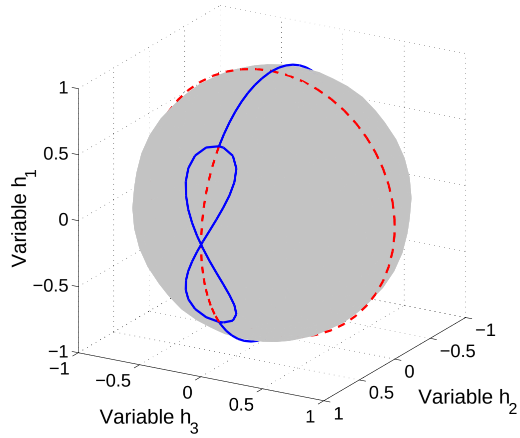

(a) Equilibria on the momentum sphere for varying h_a

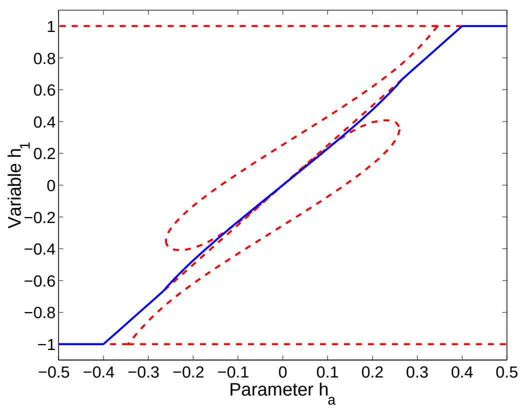

(b) h_1 *vs.* h_a

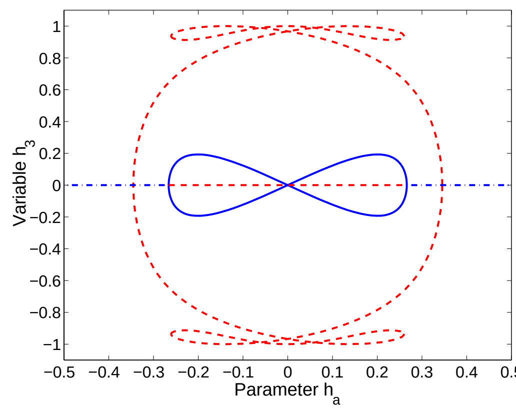

(c) h_3 *vs.* h_a

Figure 3: Equilibria for prolate gyrostat with $I_2 > I_3$, $k = 0.4$

stiffness, $0.08 < k < 0.10$, the out-of-plane equilibria branches intersect the $\hat{\mathbf{b}}_1$–$\hat{\mathbf{b}}_3$ plane equilibria in a bifurcation point. For $k = 0.08$, these branches of equilibria separate into distinct branches that both intersect $\hat{\mathbf{b}}_1$–$\hat{\mathbf{b}}_3$ plane equilibria at bifurcation points. We do not have an explicit expression for these equilibria, so we are limited to studying this transition numerically.

Another important change occurs for $0.08 < k < 0.10$. For $k = 0.1$, the nominal-spin bifurcation into the $\hat{\mathbf{b}}_1$–$\hat{\mathbf{b}}_3$ plane is a subcritical pitchfork with stable branches emanating from the nominal-spin branch of equilibria. For $k = 0.08$, the pitchfork is supercritical with unstable branches, producing a possible jump phenomenon. If a satellite is in a stable nominal spin and h_a decreases, it will reach the stability threshold, lose stability, and transition to another stable equilibrium state. For the subcritical pitchfork, the adjacent stable branch of equilibria should allow a smooth transition to the neighboring equilibrium state. For the supercritical pitchfork, there is no adjacent stable equilibrium and the system jumps to another stable state. This jump could be a substantial perturbation to the system dynamics. It is desirable to avoid such a jump, thus we seek to analytically determine the conditions for the degenerate pitchfork that marks the threshold between the subcritical and supercritical pitchforks. In the next section we use Liapunov-Schmidt reduction to determine an explicit relationship for the occurrence of the degenerate pitchfork.

BIFURCATIONS IN PARAMETER SPACE

In this section we apply Liapunov-Schmidt reduction to analytically determine conditions for the degenerate pitchfork bifurcation of the nominal spin. Complete details of these calculations are included in Reference 17.

The basic idea of Liapunov-Schmidt reduction is to reduce an n-dimensional problem,

$$\mathbf{0} = \mathbf{f}(\mathbf{z}, \alpha) \tag{35}$$

with multiple solutions to an equivalent single scalar equation. Under the assumption of a minimally degenerate case, that is, a Jacobian of rank $n-1$ at bifurcation points, the solutions of the full system, Eq. (35), may be put in one-to-one correspondence with solutions of a scalar equation

$$g(u, \alpha) = 0 \tag{36}$$

The scalar function $g(u, \alpha)$ is defined implicitly, but rarely is it possible to determine an explicit equation for $g(u, \alpha)$. However, expressions for derivatives of $g(u, \alpha)$ at the singularity are possible.

To derive the reduced equations, we first reformulate Eqs. (22–24) by translating the nominal bifurcation point to the origin, such that

$$\mathbf{f}(\mathbf{z}, \alpha) = \mathbf{f}(\mathbf{0}, 0) = \mathbf{0} \tag{37}$$

is a bifurcation point when k takes the bifurcation value $k = -b^2\varepsilon^2\lambda^3 / \left[I_1'^2 \left(I_1' + I_3\lambda \right) \right]$, given in Eq. (30).

Some distinguishing feature of the reduced function derivatives must be exploited to make use of the reduction. The qualitative properties of the local bifurcation of the full equations are equivalent to the scalar normal form for a pitchfork bifurcation

$$h(u, \alpha) = \alpha u \pm u^3 = 0 \tag{38}$$

with the $\pm$ corresponding to a subcritical or supercritical pitchfork. Equivalence of the functions g and h is demonstrated, as shown by Golubitsky and Schaeffer,[21] when $g(u, \alpha)$ at the bifurcation point satisfies

$$g = g_u = g_{uu} = g_\alpha = 0 \tag{39}$$

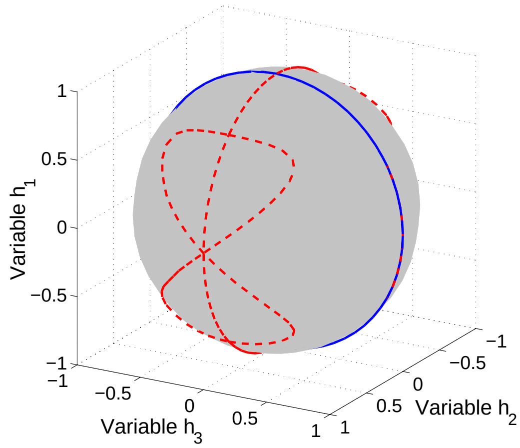

(a) Momentum sphere, $k = 0.2$

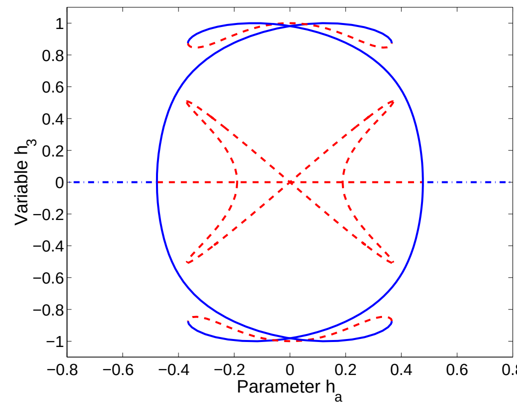

(b) h_3 *vs.* h_a, $k = 0.2$

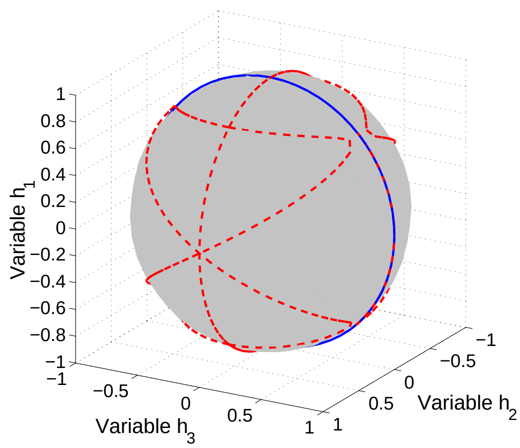

(c) Momentum sphere, $k = 0.1$

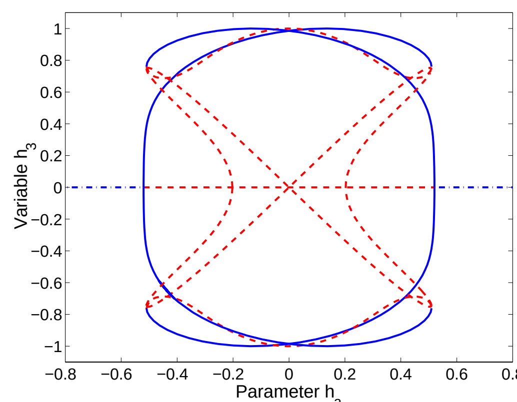

(d) h_3 *vs.* h_a, $k = 0.1$

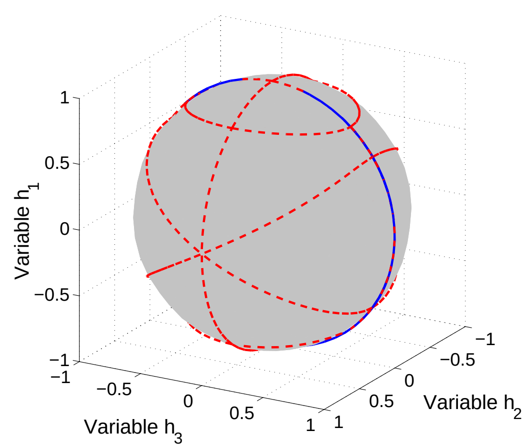

(e) Momentum sphere, $k = 0.08$

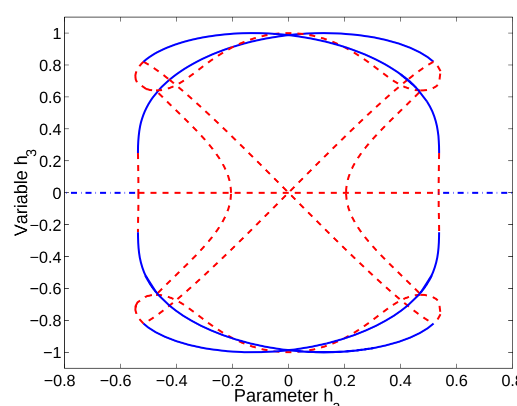

(f) h_3 *vs.* h_a, $k = 0.08$

Figure 4: Equilibria for prolate gyrostat ($I_3 > I_2$) for decreasing k

and

$$g_{\alpha u} > 0$$
$$g_{uuu} \begin{cases} > 0 & \text{subcritical} \\ < 0 & \text{supercritical} \end{cases}$$

with the latter inequality depending on the $\pm$ sign in Eq. (38).

We are interested in finding conditions on the parameters for whether the pitchfork is subcritical or supercritical. This is equivalent to finding where the sign on g_{uuu} or $g_{\alpha u}$ changes sign. Therefore, we can use Liapunov-Schmidt to determine expressions for the partial derivatives of $g(u, \alpha)$ and check the conditions on its derivatives.

We find the derivatives of $g(u, \alpha)$ using Liapunov-Schmidt reduction, and verify that at the bifurcation point

$$g = g_u = g_{uu} = g_\alpha = 0$$

The higher derivatives are

$$g_{\alpha u} = \frac{-2b\varepsilon^2 I_3^2 \lambda^3}{I_1' + I_3\lambda} \tag{40}$$

$$g_{uuu} = \frac{-3b^2\varepsilon^3 I_3^2 \lambda^4 \left[-4\varepsilon' I_1' \left(I_1' + I_3\lambda\right)^2 + b^2\varepsilon \left[\left(3I_1' + 2I_3\lambda\right)^2 + 9I_1'^2\lambda\right]\right]}{I_1' \left(I_1' + I_3\lambda\right)^2} \tag{41}$$

Examining Eq. (30), we determine that a pitchfork bifurcation only occurs for

$$-I_1'/I_3 < \lambda < 0 \tag{42}$$

For this range of rotor momentum, $g_{\alpha u} > 0$ and does not change sign. Therefore, the degenerate pitchfork is defined by the condition, $g_{uuu} = 0$, which requires

$$-4\varepsilon' I_1' \left(I_1' + I_3\lambda\right)^2 + b^2\varepsilon \left[\left(3I_1' + 2I_3\lambda\right)^2 + 9I_1'^2\lambda\right] = 0 \tag{43}$$

which can be put in the quadratic form

$$A\lambda^2 + B\lambda + C = 0 \tag{44}$$

where

$$\begin{aligned} A &= 4I_3^2 \left(b^2\varepsilon - \varepsilon' I_1'\right) \\ B &= b^2\varepsilon I_1' \left(I_1' + 12I_3\right) - 8\varepsilon' {I_1'}^2 I_3 \\ C &= {I_1'}^2 \left(9b^2\varepsilon - 4\varepsilon' I_1'\right) \end{aligned}$$

A degenerate pitchfork exists when Eq. (43) yields real values of λ, which occurs when $B^2 - 4AC > 0$. Substituting and simplifying produces the following condition for the existence of a degenerate pitchfork:

$$b^2 > \frac{16\varepsilon' I_3 \left(I_1' - I_3\right)}{\varepsilon \left(I_1' + 24I_3\right)} \tag{45}$$

For a prolate gyrostat, $I_1' < I_3$, so the degenerate pitchfork always exists.

Solving Eq. (43) for λ yields two distinct values of h_a, which indicates two possible degenerate pitchfork bifurcations. To find the corresponding values of k, we use Eq. (30) to determine the critical spring stiffness for a degenerate pitchfork:

$$k_{cr}(\lambda) = \frac{-4\varepsilon\varepsilon'\lambda^3 \left(I_1' + I_3\lambda\right)}{I_1' \left[I_1'^2\lambda + \left(3I_1' + 2I_3\lambda\right)^2\right]} \tag{46}$$

We apply these results to analytically determine the degenerate pitchfork condition for the prolate gyrostat with $\mathbf{I} = \operatorname{diag}(0.28, 0.32, 0.40)$, $I_s = 0.04$, $\varepsilon = 0.1$, $c_d = 0.1$ and $b = 0.5$. These are the same properties of the gyrostats of Figure 4, and we seek the critical spring stiffness for the degenerate pitchfork and the onset of the jump phenomenon.

Solving Eq. (43) for the two values of h_a, we use Eq. (30) to determine the corresponding values of spring stiffness, $k = 0.0900005$ and $k = -0.757886$. There is only one feasible degenerate pitchfork, with $k > 0$. However, other examples may have two distinct degenerate pitchforks. In such cases, closer examination of the corresponding bifurcations is necessary to determine the range of k to avoid the jump phenomenon. For the current example, $k > 0.090005$ produces subcritical pitchfork bifurcations of the nominal spin, avoiding the jump phenomenon. This critical value of k agrees with Figures 4(d) and 4(f), which bracket the degenerate pitchfork between $0.08 < k_{cr} < 0.1$.

The complete picture in k–h_a parameter space is given by Figure 5. The existence of the pitchfork bifurcation is determined by Eq. (42). Equation (30) determines the set of possible nominal-spin pitchfork bifurcation points. The branch of turning points near the bifurcation points, for $k < k_{cr}$, coalesces into the branch of nominal-spin pitchfork bifurcation points at the degenerate pitchfork point. This figure is qualitatively unchanged by varying ε, I_1', or I_3.

CONCLUSIONS

We characterized the equilibria of a torque-free, prolate gyrostat using analytical stability methods, numerical continuation, and analytical bifurcation techniques. Stable spins may occur with the spin axis pointing in a wide variety of directions, including out of any principal plane of the undeformed system. Multiple equilibria often exist for a given value of rotor momentum, and the global equilibria structure is affected by changing inertia properties or damper parameters. Multiple stable equilibria near the nominal spin state may exhibit a jump phenomenon, but Liapunov-Schmidt reduction of the system equations at this bifurcation point provides a method of determining conditions on the system parameters for avoiding the jump.

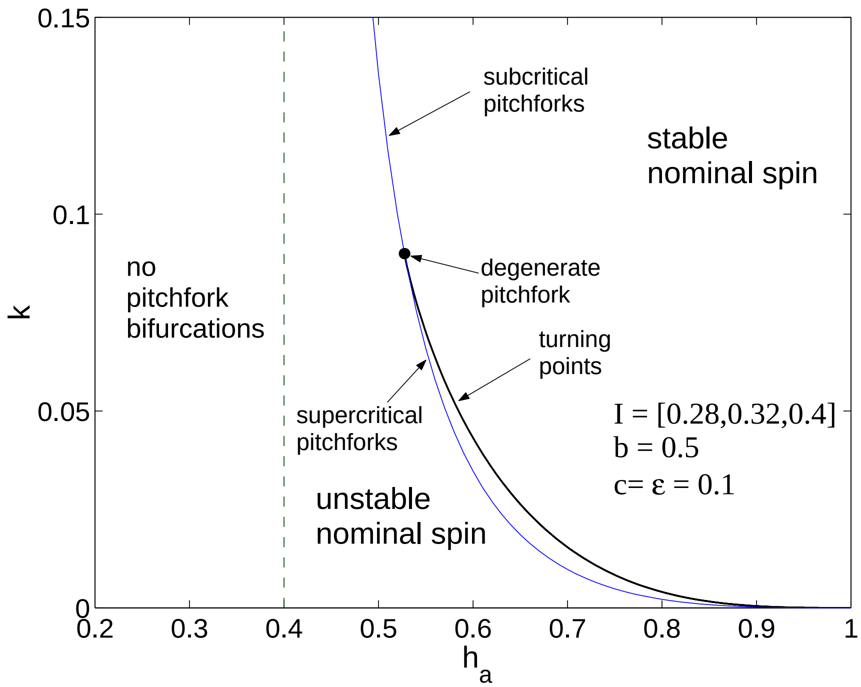

Figure 5: Nominal-spin bifurcations in k–h_a parameter space

ACKNOWLEDGMENTS

The first author has been supported by the Air Force Institute of Technology's Civilian Institutions program for Air Force Academy Faculty Preparation. The second author has been supported by the Air Force Office of Scientific Research and the National Science Foundation.

DISCLAIMER

The views expressed in this article are those of the authors and do not reflect the official policy or position of the United States Air Force, Department of Defense, or the US Government.

References

[1] Bracewell, R. N. and Garriott, O. K., "Rotation of Artificial Earth Satellites," *Nature*, Vol. 182, No. 4638, 1958, pp. 760–762.

[2] Likins, P. W., "Spacecraft Attitude Dynamics and Control — A Personal Perspective on Early Developments," *Journal of Guidance, Control, and Dynamics*, Vol. 9, No. 2, 1986, pp. 129–134.

[3] Landon, V. D. and Stewart, B., "Nutational Stability of an Axisymmetric Body Containing a Rotor," *Journal of Spacecraft and Rockets*, Vol. 1, No. 6, 1964, pp. 682–684.

[4] Iorillo, A. J., "Nutation Damping Dynamics of Axisymmetric Rotor Stabilized Satellites," In *ASME Annual Winter Meeting*, Chicago, 1965.

[5] Likins, P. W., "Attitude Stability Criteria for Dual Spin Spacecraft," *Journal of Spacecraft and Rockets*, Vol. 4, No. 12, 1967, pp. 1638–1643.

[6] Cloutier, G. J., "Stable Rotation States of Dual-Spin Spacecraft," *Journal of Spacecraft and Rockets*, Vol. 5, No. 4, 1968, pp. 490–492.

[7] Mingori, D. L., "Effects of Energy Dissipation on the Attitude Stability of Dual-Spin Satellites," *AIAA Journal*, Vol. 7, No. 1, 1969, pp. 20–27.

[8] Bainum, P. M., Fuechsel, P. G., and Mackison, D. L., "Motion and Stability of a Dual-Spin Satellite With Nutation Damping," *Journal of Spacecraft and Rockets*, Vol. 7, No. 6, 1970, pp. 690–696.

[9] Alfriend, K. T. and Hubert, C. H., "Stability of a Dual-Spin Satellite With Two Dampers," *Journal of Spacecraft and Rockets*, Vol. 11, No. 7, 1974, pp. 469–474.

[10] Hughes, P. C., *Spacecraft Attitude Dynamics*, John Wiley and Sons, New York, 1986.

[11] Levi, M.,"Morse Theory for a Model Space Structure," *Dynamics and Control of Multibody Systems, Contemporary Mathematics*, Vol. 97, American Mathematical Society, Providence, RI, 1989, pp. 209–216.

[12] Sarychev, V. A. and Sazonov, V. V., "Spin-Stabilized Satellites," *Journal of the Astronautical Sciences*, Vol. 24, No. 4, 1976, pp. 291–310.

[13] Chinnery, A. E. and Hall, C. D., "Motion of a Rigid Body with an Attached Spring-Mass Damper," *Journal of Guidance, Control, and Dynamics*, Vol. 18, No. 6, 1995, pp. 1404–1409.

[14] Hall, C. D., "Momentum Transfer Dynamics of a Gyrostat with a Discrete Damper," *Journal of Guidance, Control, and Dynamics*, Vol. 20, No. 6, 1997, pp. 1072–1075.

[15] Sandfry, R. A. and Hall, C. D., "Motion of a Gyrostat with a Discrete Damper," In *AAS/AIAA Astrodynamics Specialist Conference*, Denver, CO, Aug 2000.

[16] Schneider, C. C. and Likins, P. W., "Nutation Dampers vs Precession Dampers for Asymmetric Spinning Spacecraft," *Journal of Spacecraft and Rockets*, Vol. 10, No. 3, 1973, pp. 218–222.

[17] Sandfry, R. A., *Equilibria of a Gyrostat with a Discrete Damper*, PhD thesis, Virginia Polytechnic Institute and State University, 2001.

[18] Guckenheimer, J. and Holmes, P., *Nonlinear Oscillations, Dynamical Systems, and Bifurcations of Vector Fields*, Springer-Verlag, New York, 1983.

[19] Seydel, R., *Practical Bifurcation and Stability Analysis*, Springer-Verlag, New York, 2nd edition, 1994.

[20] Doedel, E. J., Champneys, A. R., Fairgrieve, T. F., Kuznetsov, Y. A., Sandstede, B., and Wang, X., *AUTO 97: Continuation and Bifurcation Software for Ordinary Differential Equations*, Concordia University, Montreal, Canada, 1998.

[21] Golubitsky, M. and Schaeffer, D. G., *Singularities and Groups in Bifurcation Theory, Volume I*, Springer-Verlag, New York, 1985.